View metadata, citation and similar papers at core.ac.uk
brought to you by CORE
provided by Archivio della ricerca- Università di Roma La Sapienza

Near Surface Geophysics, 2018, **16**, 67-78 doi: 10.3997/1873-0604.2017044

Focusing on soil-foundation heterogeneity through high-resolution electrical and seismic tomography

Michele Cercato* and Giorgio De Donno

Department of Civil, Constructional and Environmental Engineering (DICEA), Sapienza University of Rome, 00184 Rome, Italy

Received December 2016, revision accepted August 2017

ABSTRACT

The reconstruction of the current status of a historic building is essential for seismic safety assessment and for designing the retrofitting interventions since different safety and confidence factors have to be assumed, depending on the level of information about the subsoil structure. In this work, we present an investigation of the shallow subsurface below and around a historic building affected by differential settlements in order to define its geometry and to characterise its stiffness at low strain. To this end, we employed high-resolution electrical resistivity and seismic (both P-wave and S-wave) tomographies. A three-dimensional electrical resistivity tomography survey was performed to obtain more information about the type and the maximum depth of the building foundation. Electrical resistivity and seismic tomographies were carried out alongside the building, aimed at imaging the top soils and the near-surface geometry. The corresponding inverted models pointed out a remarkable heterogeneity of the shallow subsoil below the building, which is partly founded on a weathered layer and partly on a more rigid lithotype. This heterogeneity is probably a concurrent cause of the building's instability under both static and seismic loading. Our results demonstrate that the man-made fillings and the top soils have to be thoroughly investigated to fully understand the soil-structure behaviour. In this light, the integration of non-invasive high-resolution geophysical techniques, especially tomographic methods, has been proved to properly address the problem of imaging the shallow subsoil.

INTRODUCTION

The seismic assessment of existing structures and their response under dynamic loading is always subjected to a certain degree of uncertainty, depending on the level of knowledge of the building and ground conditions.

Two aspects play a major role when defining the seismic response of buildings, i.e., the seismic vulnerability of the structure according to exposure and the evaluation of the design criteria for the seismic displacement at the surface, comprising the contribution of local site effects on seismic motion (local seismic response).

The role of the top soils and artificial or man-made fillings on the effective seismic response, as well as the current condition of the building's foundations, is generally not considered when performing the seismic response analysis for existing structures.

For standard buildings, the design spectra associated for performance-based seismic design are evaluated on the basis of the equivalent VS30 (weighted average of the shear velocity in the first 30 m) (CEN 2003). On the other hand, seismic microzonation studies are generally focused on the geological setting, disregarding the disturbance of the geological conditions induced by the construction and the existence of the man-made fillings below the foundation level. However, the seismic properties of artificially deposited soils and fill are very important in historical centres because of their significant thickness and low stiffness, and they are too often disregarded because invasive methods may not be conveniently apply on large areas in such urban contexts. Furthermore, the level of knowledge about the building foundations is generally limited to their geometry (if schematic drawings are available) or on punctual sampling of materials and direct inspection (like trench excavations and sampling), which can be applied only on limited portions of the building. Although direct inspection and invasive tests are always required in engineering design, little attention is generally given to the great diagnostic potential achievable today by high-resolution (HR) non-destructive methods. These techniques can be useful for assessing the ground conditions, the foundation type, and the soil layering in order to plan the retrofitting interventions of existent structures.

The determination of the current status of buildings via non-invasive methods is a topic not yet covered by technical standards and, unfortunately, not yet considered as best practice among structural experts, mainly because the application of HR geophysical investigations to structural targets is a relatively new technology that has emerged in the past decades, with successful

* michele.cercato@uniroma1.it

© 2018 European Association of Geoscientists & Engineers

application not only to large infrastructures such as inspection of dams (e.g., Niederleithinger, Weller and Lewis 2012; Cardarelli, Cercato and De Donno 2014) and characterisation of river embankments (e.g., Busato *et al.* 2016) but also to standard residential buildings (Cardarelli, Cercato and Di Filippo 2007; Soupios, Loupasakis and Vallianatos 2008).

By using non-invasive geophysical techniques, our understanding of the subsoil geometry and the soil-structure interaction can be greatly improved. The geophysical prospection must be properly chosen and designed to match the required target depth and resolution as a function of the size of the building. More specifically, the experimental measurements should be focused on the following two main problems:

(1) the reconstruction of the geometry of the foundations of the building and of the underlying soil deposits, with particular focus on the man-made and artificial deposits that are not mapped in standard microzonation studies;
(2) the *in situ* determination of selected parameters characterising the shape and physical condition of the building foundations to guide the type, extent, and urgency of the seismic retrofitting intervention.

Electrical resistivity tomography (ERT) can be a flexible and reliable tool for the characterisation of the shallow subsoil (Samouëlian *et al.* 2005; Sultan and Santos 2007) and building foundations as long as three-dimensional (3D) arrays are employed (Soupios *et al.* 2007; Cardarelli *et al.* 2016). Electrical resistivity can be directly linked to changes in soil composition and saturation, as well as to the presence of buried foundations, generally exhibiting high resistivity values. This technique is rapid and low budget, and can investigate significant volumes, although, when investigating the subsoil under the building's footprint, the achievable resolution strongly decreases with depth and with the distance of the electrode array from the building perimeter. To achieve the HR required for investigating relatively small structures, it is crucial to strike a balance between the depth of investigation and the electrode spacing. However, when one has to face a multi-layered scenario with numerous resistive to conductive transitions, which is often the case in the near surface, the effective thickness of the layers can be biased and using ERT alone may not be enough to unambiguously remove the interpretation ambiguities in the inverted models. The inverted model appraisal (model resolution matrix and sensitivity (Binley and Kemna 2005)) obtained by means of the calculation of piecewise parameters is a straightforward indicator of the credibility of the inversion solutions and may help in avoiding over-interpretation of inversion artefacts.

In an effort to reduce the degree of uncertainty, geoelectrical methods have often been linked to geotechnical data (Sopuios *et al.* 2008; Sudha *et al.* 2009), obtained under static loading and up to permanent deformation using, for instance, standard penetration test (SPT) or cone penetration test (CPT) investigations (Paasche *et al.* 2013).

Seismic methods have a great diagnostic potential for engineering applications since variations in compressional (P-wave) and shear (S-wave) seismic velocities are associated to analogous variations in shear strength and soil stiffness at low strain. In particular, for engineering applications, seismic refraction tomography (SRT) has now superseded the conventional refraction interpretation that works only when seismic velocity is continuously increasing with depth (Pelton 2005). The combination of both P-wave and S-wave models can lead to the estimation of the Poisson's ratio directly connected to porosity and elastic displacement calculations (Lancellotta 2009). The diagnostic potential of the seismic methods strongly depends on the site conditions and ground response, particularly to achieve the HR required for a small-scale survey.

The integration of HR seismic and electrical tomography applied to the diagnosis of the stability of existing buildings is the main goal of this work, which has been divided into five main steps as follows:

1. definition of the reference geological setting through two-dimensional (2D) ERT and seismic tomography investigations executed in the surroundings of the building;
2. identification of the geometry of the soil foundations of the building using 3D ERT arrays;
3. focus on the top soil by integrating 2D ERT and seismic tomography investigations;
4. definition of a representative model of the shallow subsoil and soil foundations to be used both for static and seismic verifications;
5. validation of a geophysical model through excavations and geotechnical investigations.

This experimental procedure has been applied to a historical building, near the town of Rieti (Central Italy), which has been damaged by the recent seismic earthquakes in Central Italy (2009 and 2016).

EXPERIMENTAL PROCEDURE

Site description

The study site is located near the town of Rieti (Central Italy), around 80 km north of Rome, at a distance of 40 km from the epicentre of the major earthquake (M_w=6.0) occurred in August 2016. The structure under examination, built in 1910, is a two-floor masonry building (Figure 1a) used as a national research centre for agricultural studies.

The geophysical survey discussed in this paper was conducted in 2015 before the last seismic sequence. At the time of the geophysical survey, the building showed numerous cracks and fractures detected on the load-bearing walls and possible differential settlements phenomena occurred in the soil foundations. From a preliminary visual inspection, thick cracks were identified on the southern load-bearing walls (Figure 1b), related to the 2009 L'Aquila earthquake. The foundations of the building, inferred from the available historical information, are supposed

to be equally spaced masonry walls (strip footings) about 1 m wide and probably extended up to a depth ranging from 1.5 to 2.5 m.

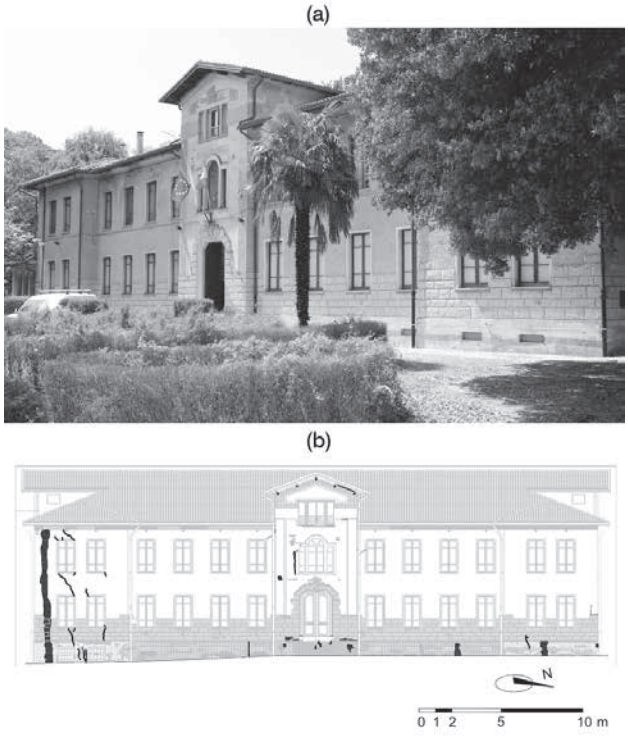

Figure 1 (a) Main building of the research centre under investigation. (b) Front view of the building where cracks in the southern load-bearing walls are marked with black lines.

The geological background is characterised by fractured carbonate units, which comprise the Mts. Sabini-Reatini ridges, belonging to the Meso-Cenozoic units of the Umbro–Sabina domain, where a groundwater circulation is present. In the seismic microzonation map of the municipality of Rieti, the site under investigation is located within the travertine outcropping area, with variable soil thickness above the travertine bedrock.

Data acquisition and processing

Figure 2 presents a plan view (Figure 2a) and a cross section (Figure 2b) of the building reporting the entire geophysical survey. The 2D tomographic investigations (electrical resistivity and P- and SH-wave seismic tomographies) are located along three lines (L1, L2, and L3 in Figure 2). With reference to the main steps described in the introduction, we used the L2 and L3 lines for reconstructing a geophysical model of the undisturbed shallow subsoil, whereas a more focused HR survey was executed on the L1 line, for assessing the soil conditions affecting the building. Three-dimensional ERT data were acquired near the building on the C- and L-shaped arrays (Figure 2) for imaging the shape of the foundations. Elevations and depths are all expressed with respect to a zero-reference point (position of electrode/geophone 1 of the L1 line). There is a noticeable elevation change within the study area from south to north (around 2.5 m).

In the late spring of 2017, the excavation of two trenches (cross points in Figure 2) and the execution of an SPT (reverse triangle point) allowed us the validation and helped the geological interpretation of the geophysical results.

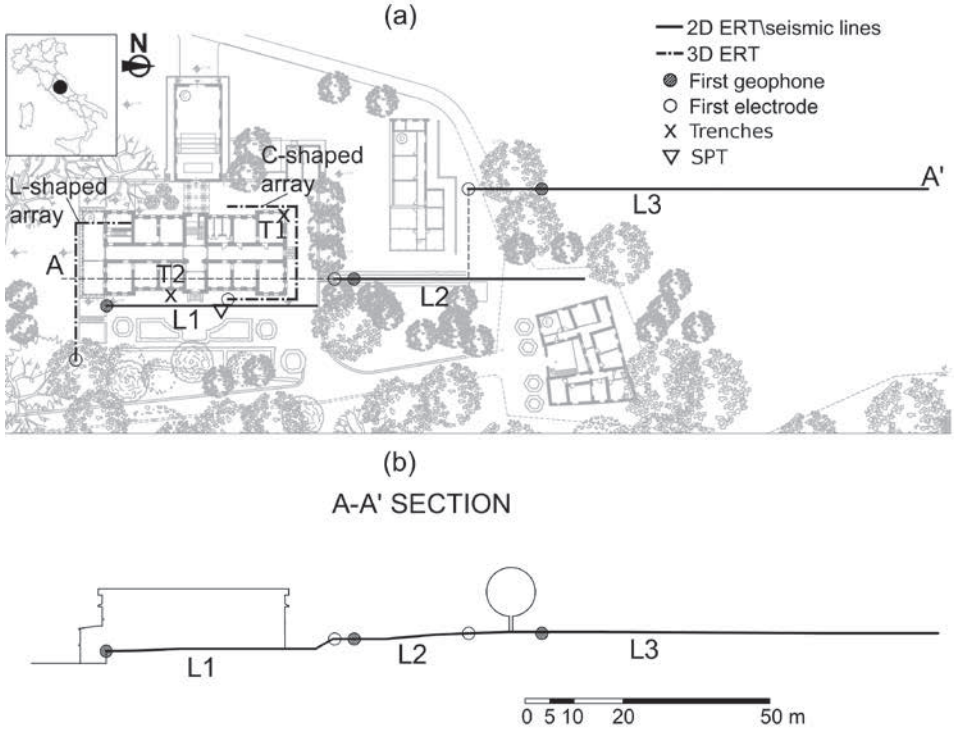

Figure 2 (a) Location of the geophysical and geotechnical survey at the site under investigation. (b) A–A' cross section of the study site.

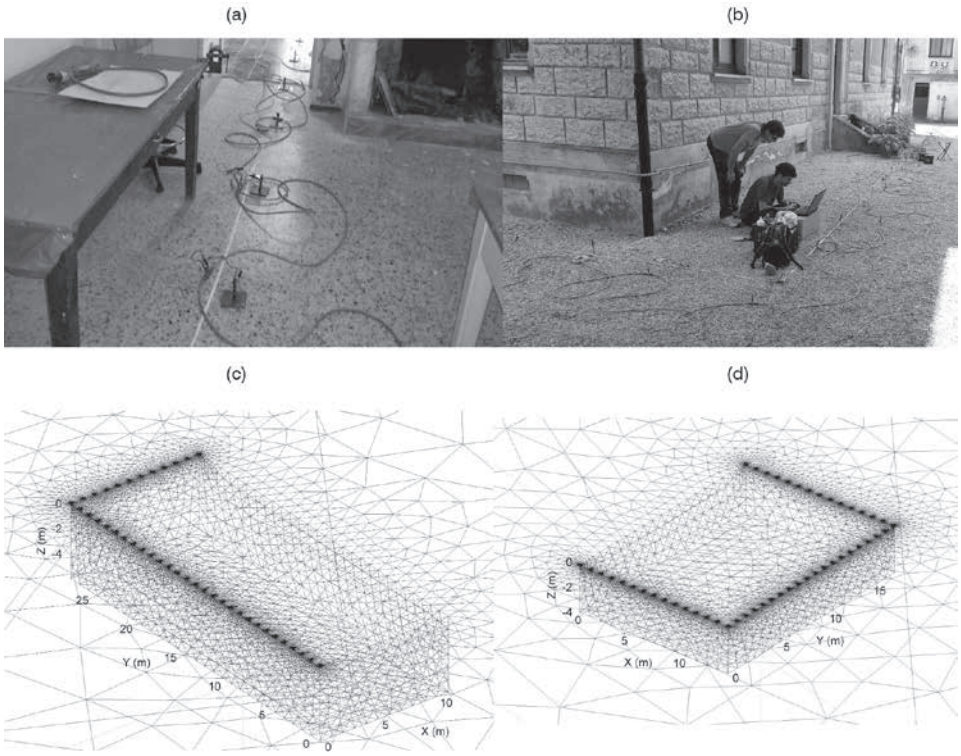

Figure 3 Three-dimensional electrical acquisition on (a) the L-shaped and (b) the C-shaped arrays. Finite-element meshes used for forward computation for (c) the L-shaped and (d) the C-shaped arrays.

Figure 4 (a) P-wave and (b) SH-wave acquisition on the L1 line.

Electrical resistivity tomography

Two-dimensional ERT data were acquired using a 48-electrode IRIS Instruments SyscalPro48 using a combination of dipole–dipole and Wenner–Schlumberger configurations with stainless steel electrodes spaced apart by 1 m (L1, L2) and 2 m (L3). Three-dimensional acquisitions were performed by means of a dipole–dipole configuration on L-shaped (29 × 11 electrodes, Figure 3a) and C-shaped (14 × 18 × 14 electrodes, Figure 3b) arrays. These arrays combine robust signal strength with satisfying resolution and good depth of investigation. The ERT measures were inverted using the VEMI algorithm (De Donno and Cardarelli 2017a) built within the EIDORS environment (Adler and Lionheart 2006). This algorithm is capable of performing both 2D and 3D inversions by solving the forward problem with a finite-element approximation of Laplace's equation governing the physical problem (De Donno and Cardarelli 2014). The inversion is carried out using a Gauss–Newton formulation where the optimum damping factor is chosen at each iteration (De Donno 2013). An example of finite-element meshes (built for forward solution, where also the finite length of the electrodes is taken into account) is shown in Figure 3c (L-shaped array) and in Figure 3d (C-shaped array). Although it is possible to add *a priori* information to the inversion process; in

this particular case, we made no preliminary assumption on the soil layering.

Seismic refraction tomography

Seismic tomography data were recorded employing a 48-channel system of 4.5-Hz vertical (P-wave) and 8-Hz horizontal (SH-wave) geophones at 1-m spacing. The source was a 7-kg hammer source on a steel plate (P-wave, Figure 4a) and a light-weight aluminium source (SH-wave, Figure 4b) using a Geometrics Geode seismograph at a sampling rate of 0.125 ms. Both acquisitions were performed with a geophone streamer, made up by abrasion-resistant steel tripod plates connected and towed by a high tensile-strength band. For each shot gather, the first arrivals were manually picked, and travel-time inversion was performed using the algorithm described in Cardarelli and de Nardis (2001), employing the linear travel-time interpolation method for ray tracing (Asakawa and Kawanaka 1993) and the iterative biconjugate gradient algorithm for travel-time inversion (Cardarelli and Cerreto 2002). This software can also deal with velocity inversions. The initial model has been inferred from the soil layering obtained by resistivity inversion.

In Figure 5, an example shot gather is illustrated for the seismic tomography L3 line, where good-quality first arrivals could be picked, as shown in Figure 5a (P-wave) and Figure 5b (SH-wave). For SH-wave, picking was facilitated by overlapping two opposite-polarity records at each shot location (Figure 5b). The prevalent frequency content of the seismic signals inferred from the Fourier amplitude spectra of the seismograms (Figures 5c and d), after a few near-offset traces, is not particularly high, i.e., around 150–200 Hz for P-wave and 70–120 Hz for SH-wave.

RESULTS

Geological setting

The reference geological setting was evaluated through the combined analysis of the tomographic inversions (ERT and SRT) on the L2 and L3 lines. The L2 line (elevation of about 2 m above the main building) consisted only of P-wave data.

The ERT inverted model of the L3 (Figure 6a) line exhibits three main layers: two conductive layers (resistivity $\rho < 20$ Ωm for the shallower layer and about 50–60 Ωm for the middle layer) overlying a resistive formation ($\rho > 400$ Ωm), dipping northwards up to a maximum depth of 17–18 m. The resistive layer may correspond to the travertineous formation. The L2 line (Figure 6b) shows a slightly different behaviour: the inverted section is a four-layer model where a resistive layer ($\rho = 200$–400 Ωm) can be seen between the two conductive units. The shallower conductive layer ($x = 0$–20 m) cannot be interpreted as a natural lithotype because it is the result of a rearrangement of the slopes in this zone. Overall, the model confirms the resistivity range for the deeper units (travertine and overburden) while a shallow resistive layer is now visible that may be related to a coarse-grained overburden.

The L3 seismic tomography lines (P- and SH-waves) are displayed in Figures 7a and 7b, respectively. The subsoil layering inferred from ERT is confirmed, adding information about the elastic properties at low strain of the lithological units. In fact, the conductive shallow layer is associated with low P-wave (350–550 m/s) and SH-wave (150–250 m/s) velocities, indicative of a weathered material. Below, the P- and SH-wave velocities increase progressively up to 850 and 300 m/s, respectively. Since the maximum depth of these models is 9 m, the travertineous unit ($V_P > 1000$ m/s; $V_S > 400$ m/s) is reached only in the left (southern) side of the model ($x = 0$–5 m) in Figure 7a, corresponding

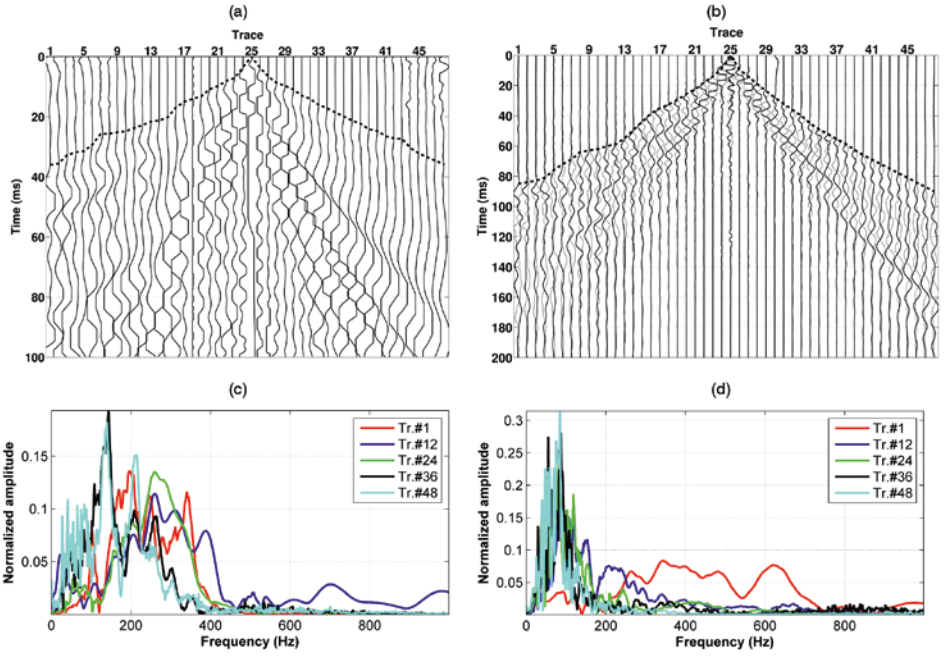

Figure 5 Example P- and SH-wave shot gathers. (a) Raw P-wave seismogram with picked P-wave arrivals (dashed line). (b) Raw SH-wave seismogram with picked S-wave arrivals (dashed line). For each receiver position, the two traces corresponding to the opposite shot directions (solid black line and solid grey line, respectively) are superimposed to enhance picking by phase opposition of the polarised shear wave. (c) Fourier amplitude spectrum of selected traces for the P-wave seismogram in Figure 5a. (d) Fourier amplitude spectrum of selected traces for the SH-wave seismogram in Figure 5b.

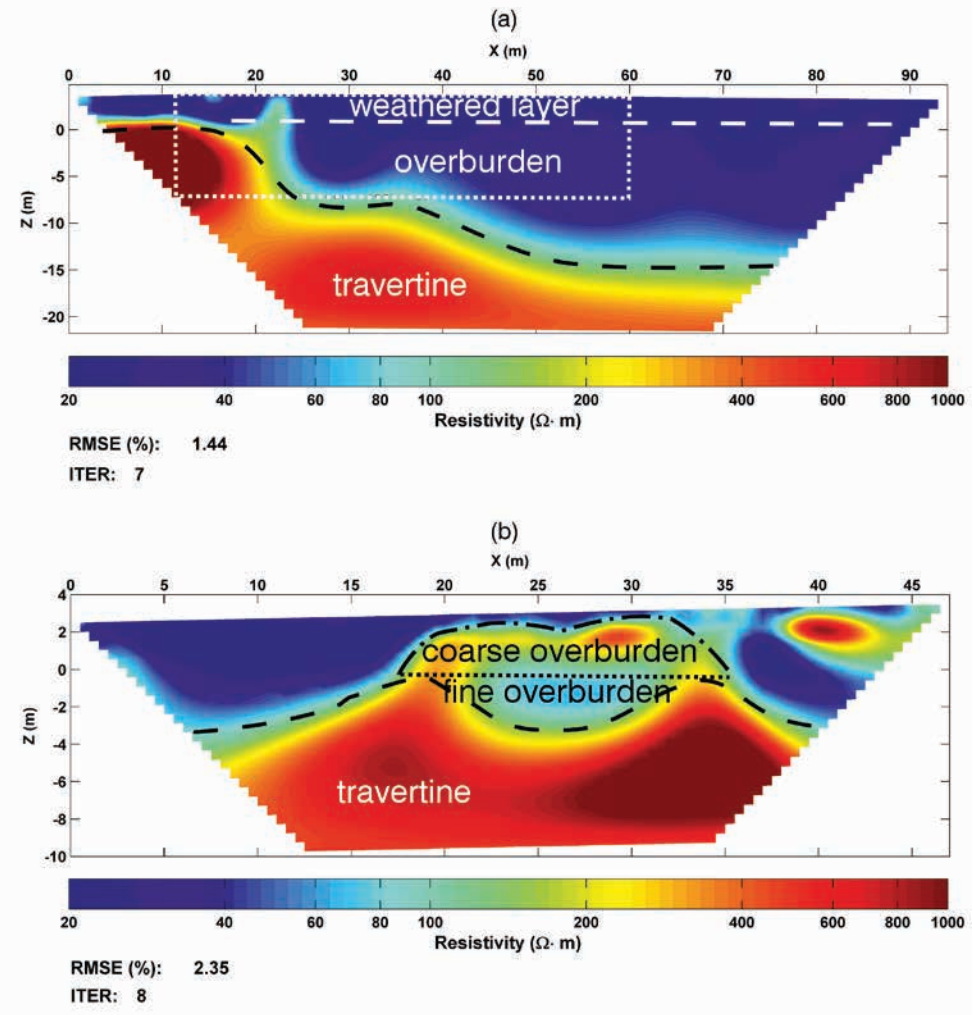

Figure 6 Two-dimensional ERT inverted models of (a) the L3 and (b) the L2 lines. The location of the seismic tomography model is marked with a white dotted line. The interfaces between different layers are represented by dashed, dotted, and dash-dot black lines.

to x = 15–20 m in Figure 6a, where it is found at shallower depths, also by ERT.

The initial model for inversion of the P-wave dataset for the L2 line (Figure 8) was set up on the basis of the layer geometry inferred from ERT inversion because it is likely to have a velocity inversion given the high heterogeneity in the shallow subsurface. The final model (root-mean-square error (RMSE) = 12.2%) displays low- to high-velocity transitions that correspond to the interfaces detected by the ERT inverted model.

The investigation of the virtually undisturbed geological setting has pointed out a remarkable variability of the depth of the travertine unit within the site, together with relatively poor elastic characteristics of the shallow sediments and the travertine itself. The effective layout of the subsoil, inferred from the combined use of the electrical and seismic tomographic models, has been set as the geological reference model for the further investigations to be performed near the building.

Building foundation

The second step in the evaluation of the soil-structure system is the identification of the type and shape of the building foundations using 3D ERT. This step is needed due to the unavailability of the design plans of the building's foundations. The results of the 3D ERT inversion are reported in Figure 9 in terms of a volumetric representation of the high-resistivity areas corresponding to the foundation walls (resistivity > 400 Ωm) for both arrays (L-shaped in Figure 9a and C-shaped in Figure 9b). The superposition of the main building's footprint on the electrical model is consistent in both cases, and the interpretation of the resistivity anomalies in terms of the geometry of the foundation elements is accurate. In fact, the highest resistivity values are retrieved along both the x- and y-directions, indicating that the foundations could be strip footings located underneath the load-bearing walls. Since the resolution of an ERT survey strongly depends on the array choice, particularly for a 3D investigation, we mapped in Figures 9c and 9d the cumulative sensitivity (Park and Van 1991; De Donno and Cardarelli 2017b) of the two electrode configurations (C- and L- shaped, respectively). Overall, sensitivities lower than 10^{-5} can be associated to low credibility zones (Nguyen *et al.* 2009). Consequently, the volumetric representations shown in Figures 9a and 9b were restricted only to zones with sensitivities higher than 10^{-5}. Finally, the ERT reconstruction has been compared with the supposed location of the

foundation walls (dotted lines). The good correspondence between ERT models and the expected location of the walls confirms that foundations are strip footings that might be extended up to 2–2.5 m and therefore interact only with the shallower part of the subsoil.

Top soil and the artificially deposited layer

Given the geological stetting and the type of foundations observed above, we further investigate the top soil through HR tomographic reconstruction focused on the building area (L1). Figure 10 shows the results of the tomographic inversion of electrical resistivity data acquired along the L1 line, where the building profile is superimposed for clarity. The inverted model indicates a four-layer configuration, where the travertine is recovered, under the building, at a depth of 8 m ($\rho > 400$ Ωm). Above the calcareous formation, we recovered the same layering (conductive–resistive–conductive), as in the L2 line. Therefore, we can associate the deeper conductive units to a fine overburden (depth of 5–8 m, ρ = 60–70 Ωm) and the shallower ones to a weathered material (depth of 0–2 m, ρ = 20 Ωm). The latter layer is seen only in the first part of the model (x = 0–22 m), whereas in the second part (x = 22–34 m), the resistive formation emerges (ρ = 200–400 Ωm), probably related to the coarse-grained sediments seen on the L2 line (Figures 6b and 8).

Given this layout, it is likely to have a velocity inversion in the corresponding seismic profile. We add this information in the initial model for inversion of seismic refraction data. The starting seismic model for inversion was calibrated on the layer geometry identified by ERT, with P- and SH-wave mean velocities inferred from the L1 SRT model, whereas for the middle resistive formation (coarse-grained overburden), values of 700 and 300 m/s are assigned to P- and SH-wave velocities, respectively. Results of SRT inversion are shown in Figures 11a (P-wave) and 11b (S-wave). Both models exhibit relatively low values of RMSE (11.4% and 9.9%). The moderately stiff travertine (V_P > 1000 m/s; V_S > 400 m/s) emerges only in the right part of the models (outside the building), whereas elsewhere, it is located at a depth of about 8 m (Figure 11). The layer geometry (shape and depth of the interfaces) is comparable with that recovered by ERT, and the final models confirm the velocity inversion at a depth of around 5 m. The S-wave model exhibits lower resolution with respect to the P-wave one, mainly due to an increase level of uncertainty in the picking of travel times. In fact, we have less ray paths for S-wave with respect to the P-wave. Since we aimed to fit data with a comparable error level, this issue leads to a flatter final model, as compared with the P-wave one.

Validation of the geophysical model

At the end, the geophysical results were validated by the aid of direct excavations of the shallow portion of the subsoil and an

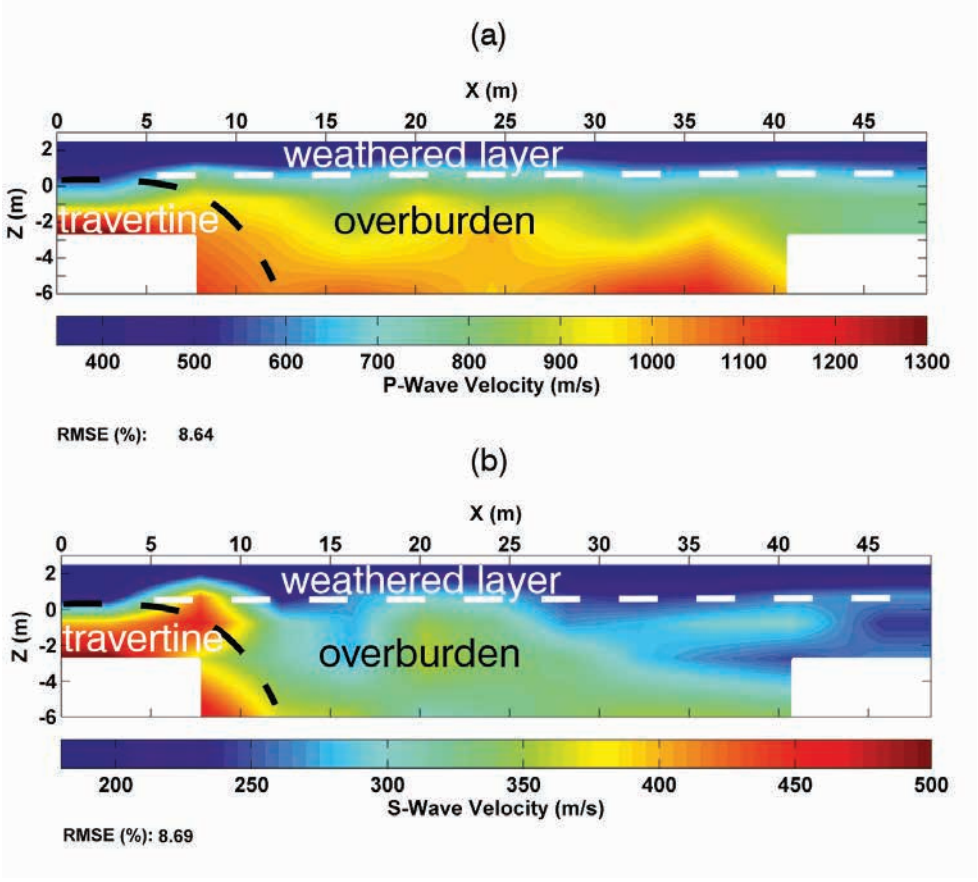

Figure 7 SRT inverted models of the L3 line. (a) P-wave model. (b) SH-wave model. The interfaces between different layers are represented by dashed black and white lines.

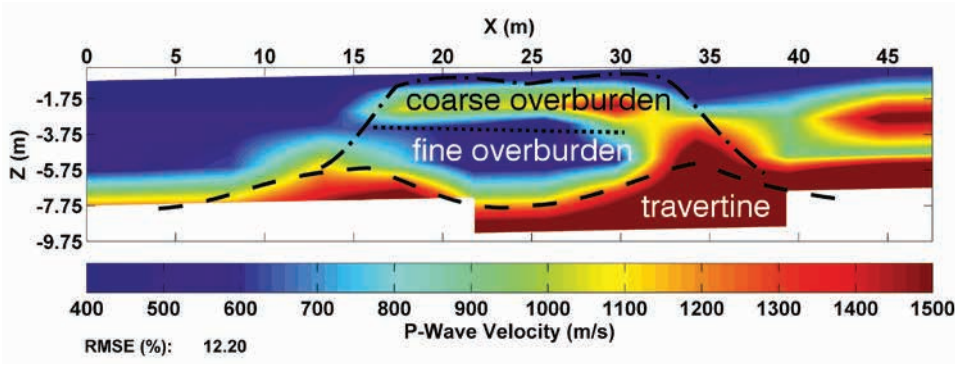

Figure 8 SRT P-wave inverted models of the L2 line. The interfaces between different layers are represented by dashed, dotted, and dash-dot black lines.

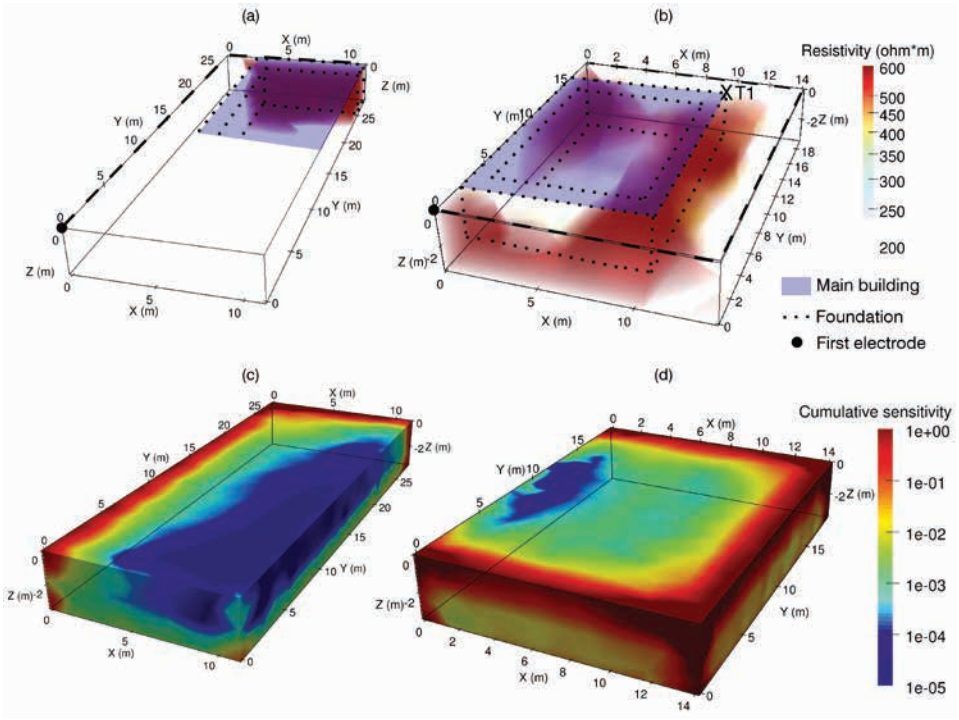

Figure 9 Volumetric representation of the 3D ERT inverted models for detecting foundations. (a) L-shaped array model. (b) C-shaped array model. Only values higher than 400 Ωm are represented. The location of the building foundations (dotted lines) is superimposed to the models. Cumulative sensitivities for (c) the L-shaped and (d) the C-shaped arrays.

SPT investigation. The excavations, located as shown in Figure 2a (cross points), were performed using trenches extended up to a depth of 2.5 m (Figures 12a and 12b), where the lower bound of the foundation was reached accordingly to the ERT evidence. After a visual inspection of the trenches, we can confirm the presence of the foundation walls along the perimeter of the building (Figures 12a and 12b). Additionally, Figure 12a highlights the presence of masonry structures that extend laterally beyond the building perimeter: this is consistent with the high resistivity values shown in the resistivity model in Figure 9b outside the building footprint (y > 16 m in Figure 9b).

Results of the SPT (reader can refer to Figure 2a for its location) are reported in Figure 12c (blow counts as a function of depth). The blow counts were also superimposed to the ERT and SRT models (Figures 10 and 11, respectively) to give a straightforward validation of the geophysical results. The combined analysis of the results confirms the four-layer configuration of the subsoil, where the depths of the transitions between high and low SPT blow counts are similar to those of the interfaces detected by the employed geophysical methods. The blow counts pertaining to the travertineous unit (z > 8 m) can be associated to a medium-stiff lithotype according to normally adopted criteria (Bowles 1996).

DISCUSSION

The HR inverted models pointed out that the building is founded on a highly heterogeneous subsoil. The conductive weathered layer, extended up to the middle of the building, has very poor elastic properties (V_P = 350 m/s and V_S=150 m/s), leading to a Poisson's ratio around 0.35–0.4. The resistive lithotype emerging on the northern part of the building (coarse-grained sediments) is more rigid, with V_P = 600–700 m/s and V_S=250–350 m/s (Poisson's ratio of 0.3–0.35). Since the building is founded on shallow foundations (0–2 m), it is likely that this heterogeneity is a concurrent cause of the building's instability.

Overall, the two tomographic models (electrical resistivity and seismic refraction) have fulfilled the HR requirement for

small-scale engineering applications, although with differences in terms of depth of investigation and loss of resolution with depth. Electrical methods investigate remarkable depths compared with the array spread, although with resolution loss with depth. On the other hand, the quality of the seismic tomography inversion is affected by the high attenuation of the body waves with distance for such low-stiffness materials, which results in a tomographic reconstruction limited to moderate offsets, leading to small investigation depths. For these reasons, it is advantageous to integrate the results of electrical and seismic tomography because of their complementarity.

In our case study, there are no significant differences between P- and SH-wave models in terms of layer geometry so that the investigated subsurface exhibits a low value of water saturation,

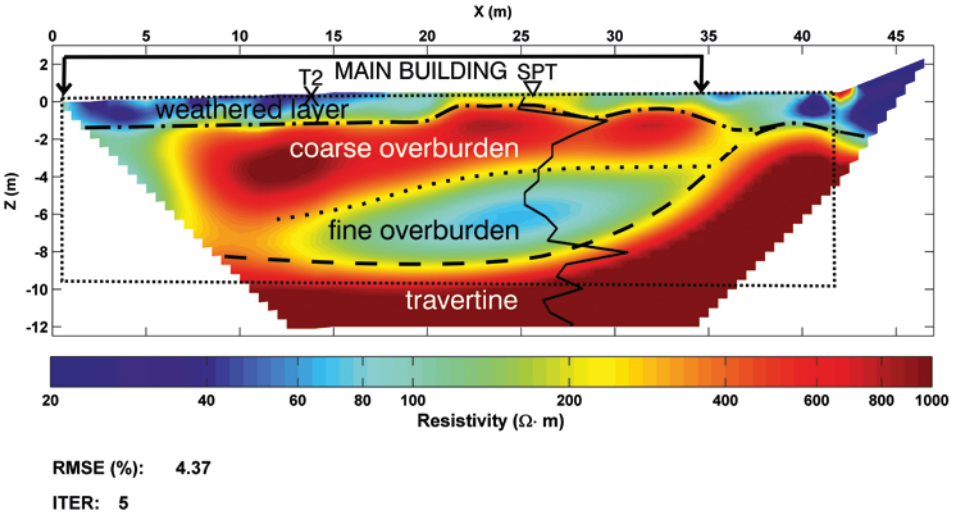

Figure 10 Two-dimensional ERT inverted model of the L1 line. The location of the seismic tomography model is marked with a black dotted line. The interfaces between different layers are represented by dashed, dotted, and dash-dot black lines. The result of the SPT shown in Figure 13c is superimposed with a black solid line.

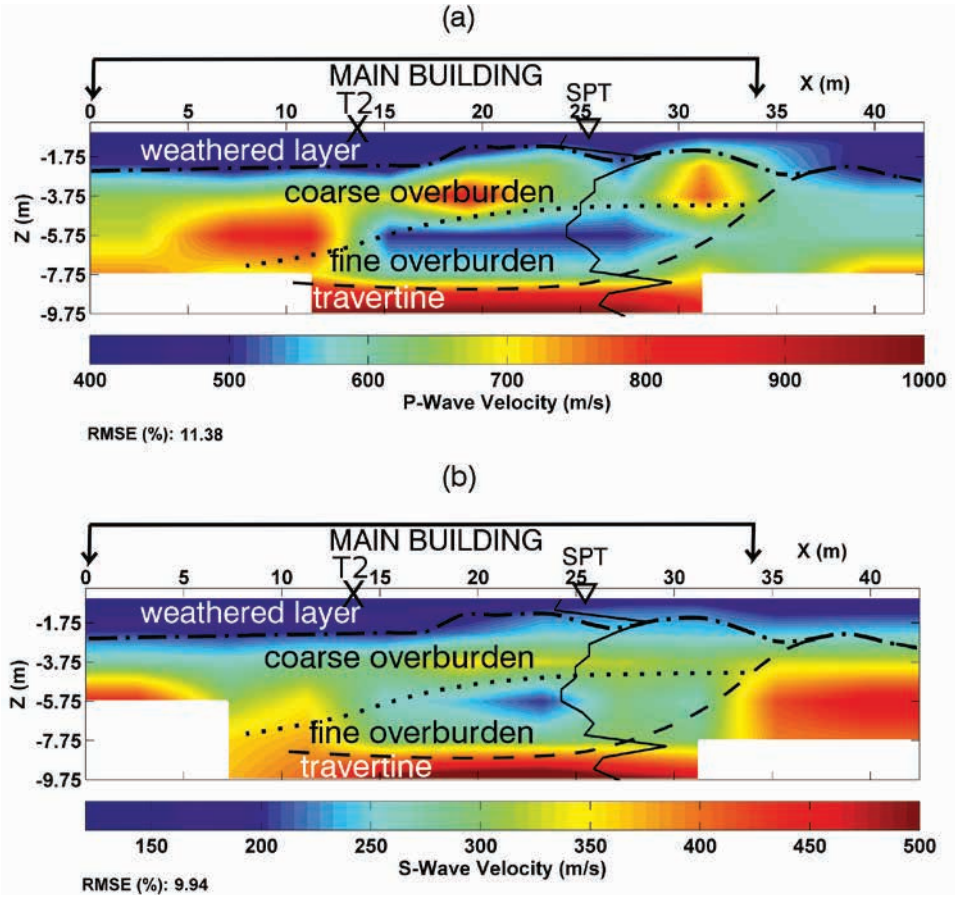

Figure 11 SRT inverted models of the L1 line. (a) P-wave model. (b) SH-wave model. The interfaces between different layers are represented by dashed black and white lines. The result of the SPT shown in Figure 13c is superimposed with a black solid line.

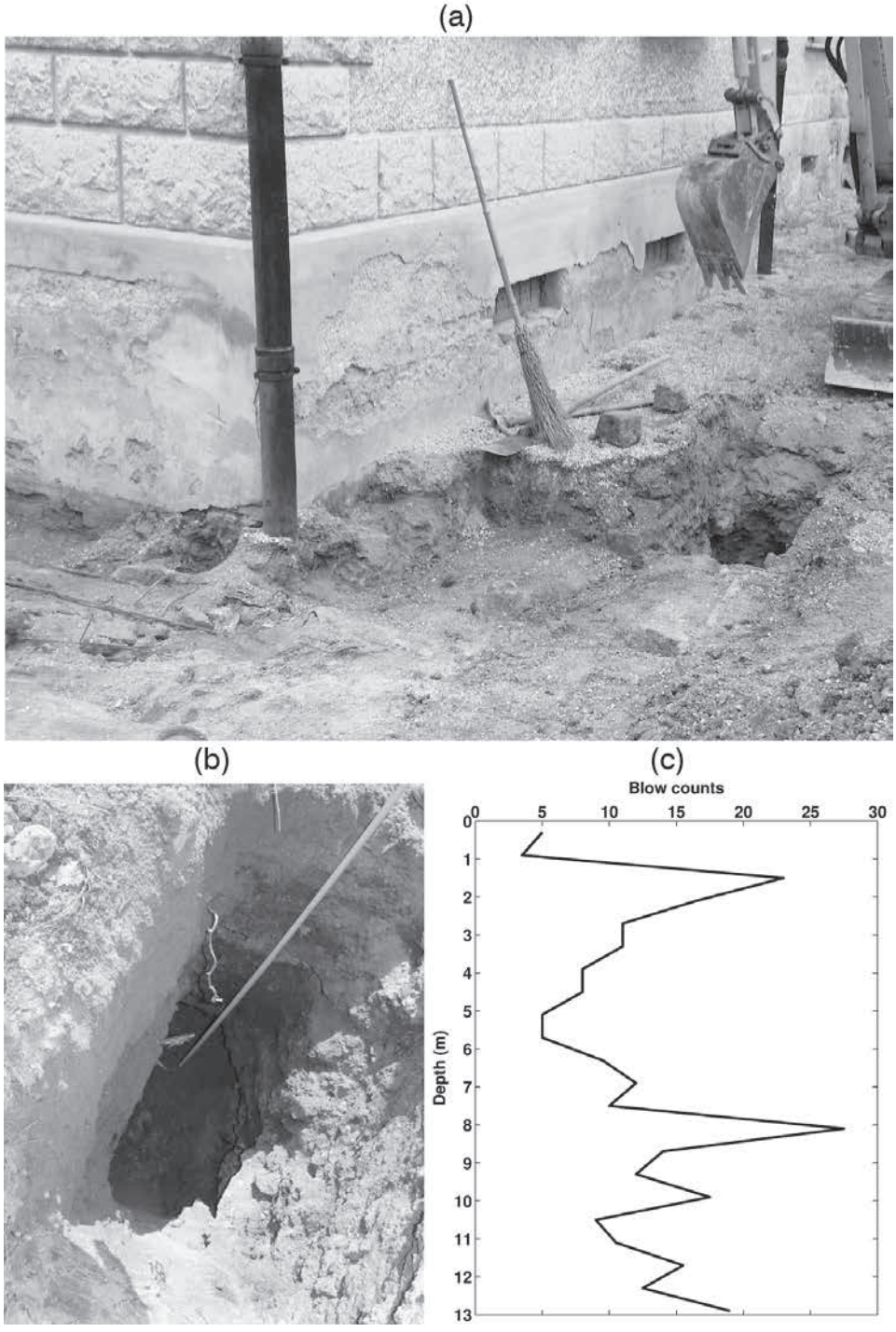

Figure 12 Trenches excavated for the validation of geophysical results marked as (a) T1 and (b) T2 in Figure 2a. (c) Results of the SPT investigation expressed in terms of blow counts as a function of depth.

with the water table being estimated at a depth larger than 20 m at the time of the survey.

The S-wave measurements provide additional benefits: the capability of pointing out low-stiffness areas of the top soil (independently from the water content) and use of the shear velocities for immediate use in seismic verification.

In the case of historic buildings, the construction details are often unknown. The subsoil geometry assessment and soil foundations need to be investigated as a whole system. To this aim, the 3D geoelectrical survey has an enormous diagnostic potential due to its capability of pointing out the type and the geometry of the buried foundations and to its versatility in the array shape, which allows the method to be employed for highly irregular buildings.

An accurate geophysical reconstruction can also improve the cost effectiveness of the invasive tests by reducing the number of boreholes required for the geological and geotechnical

characterisation. In this case study, *a posteriori* direct inspections (trenches and SPT investigation) confirmed the geophysical reconstruction in terms of the type of foundation, layer geometry, and lithotypes.

CONCLUSION

In this research we have investigated the potential and limits of an experimental procedure encompassing HR tomographic reconstruction of electrical and seismic models, for assessing the causes of instability due to spatially varying seismic displacement below a historical building.

Firstly, a detailed reconstruction of the *in situ* geological condition was achieved through a combined use of ERT and SRT, where the depth of the travertineous layer below the overburden varies significantly within the study site. The range of variation of the main geophysical parameters (electrical resistivity and P- and S-wave velocities), inferred from these models, was set as a reference for tuning the results obtained from the geophysical survey performed near the building.

The building foundations, inferred by customised 3D ERT arrays, are strip footings located underneath the load bearing walls and extended up to 2 m in depth, therefore affecting only the shallow depths. The soil above the travertineous bedrock was investigated in detail using both HR electrical and seismic (P- and S-wave) tomographies. The inverted models clearly indicate the heterogeneity of the shallow subsoil along the building, which is partially founded on a weathered layer and partially on a more rigid lithotype related to coarse-grained sediments. Therefore, differential seismic amplification along the building may be caused by the heterogeneity of the shallow subsoil. In this light, the role of artifcially deposited soils and fillings can be very relevant for shallow foundations.

The proposed experimental procedure is rapid, low-budget, and completely non-invasive; it can be fully or partially executed according to the resolution required, the available budget, and the desired target.

ACKNOWLEDGEMENTS

This work was funded by Sapienza University of Rome under Ateneo Grant 2013 prot. C26A135KYX (scientific coordinator: Michele Cercato). Edoardo Currà and Alessandro D'Amico (Sapienza University of Rome) are thanked for the accurate architectural survey and for fruitful discussion about the building. Dr. Stefano De Blasi is thanked for the results of direct excavations and standard penetration test. Francesco Pugliese (Sapienza University of Rome) is thanked for his technical support on data acquisition. The core findings of this paper were presented at the 22nd European Meeting of Environmental and Engineering Geophysics (Cercato and De Donno 2016).

REFERENCES

Adler A. and Lionheart W.R. 2006. Uses and abuses of EIDORS: an extensible software base for EIT. *Physiological Measurement* **27**, S25.

Asakawa E. and Kawanaka T. 1993. Seismic ray tracing using linear travel time interpolation. *Geophysical Prospecting* **41**, 99–111.

Binley A. and Kemna A. 2005. DC resistivity and induced polarization methods. In: *Hydrogeophysics*, pp. 129–156. Dordrecht, Netherlands: Springer.

Bowles J.E. 1996. *Foundation Analysis and Design*, 5th edn, pp. 135–166. Singapore: McGraw-Hill.

Busato L., Boaga J., Peruzzo L., Himi M., Cola S., Bersan S. *et al.* 2016. Combined geophysical surveys for the characterization of a reconstructed river embankment. *Engineering Geology* **211**, 74–84.

Cardarelli E. and De Nardis R. 2001. Seismic refraction, isotropic anisotropic seismic tomography on an ancient monument (Antonino and Faustina temple AD 141). *Geophysical Prospecting* **49**, 228–240.

Cardarelli E. and Cerreto A. 2002. Ray tracing in elliptical anisotropic media using linear travel-time seismic interpolation (LTI) method applied to travel time seismic tomography. *Geophysical Prospecting* **50**, 55–72.

Cardarelli E., Cercato M. and Di Filippo G. 2007. Assessing foundation stability and soil-structure interaction through integrated geophysical techniques: a case history in Rome (Italy). *Near Surface Geophysics* **5**, 141–147.

Cardarelli E., Cercato M. and De Donno G. 2014. Characterization of an earth-filled dam through the combined use of electrical resistivity tomography, P-and SH-wave seismic tomography and surface wave data. *Journal of Applied Geophysics* **106**, 87–95.

Cardarelli E., De Donno G., Scatigno C., Oliveti I., Martinez M.P. and Prieto-Taboada N. 2016. Geophysical and geochemical techniques to assess the origin of rising damp of a Roman building (Ostia Antica archaeological site). *Microchemical Journal* **129**, 49–57.

CEN 2003. EuroCode 8: design of structures for earthquake resistance. Part 1: general rules, seismic actions and rules for buildings. Draft 6. Brussels, Belgium: European Committee for Standardization.

Cercato M. and De Donno G. 2016. Focusing on soil foundation heterogeneity through high-resolution tomography. *22nd European Meeting of Environmental and Engineering Geophysics*, Barcelona, Spain, September 4–8, 2016.

De Donno G. 2013. 2D tomographic inversion of complex resistivity data on cylindrical models. *Geophysical Prospecting* **61**, 586–601.

De Donno G. and Cardarelli E. 2014. 3D complex resistivity tomography on cylindrical models using EIDORS. *Near Surface Geophysics* **12**, 587–598.

De Donno G. and Cardarelli E. 2017a. VEMI: a flexible interface for 3D tomographic inversion of time- and frequency-domain electrical data in EIDORS. *Near Surface Geophysics* **15**, 43–58.

De Donno G. and Cardarelli E. 2017b. Tomographic inversion of time-domain resistivity and chargeability data for the investigation of landfills using a priori information. *Waste Management* **59**, 302–315.

Lancellotta R. 2009. *Geotechnical Engineering*. Taylor and Francis.

Nguyen F., Kemna A., Antonsson A., Engesgaard P., Kuras O., Ogilvy R. *et al*. 2009. Characterization of seawater intrusion using 2D electrical imaging. *Near Surface Geophysics* **7**, 377–390.

Niederleithinger E., Weller A. and Lewis R. 2012. Evaluation of geophysical techniques for dike inspection. *Journal of Environmental and Engineering Geophysics* **17**, 185–195.

Paasche H., Rumpf M., Hausmann J., Fechner T., Werban U., Tronicke J. *et al.* 2013. Advances in acquisition and processing of near-surface seismic tomographic data for geotechnical site assessment. *First Break* **31**, 59–65.

Park S.K. and Van G.P. 1991. Inversion of pole-pole data for 3D resistivity structure beneath arrays of electrodes. *Geophysics* **56**, 951–960.

Pelton J.R. 2005. Near-surface seismology: surface-based methods. In: *Investigations in Geophysics* (ed D.K. Butler) *Near-Surface Geophysics* **13**, 219–263. Tulsa, OK: Society of Exploration Geophysicists.

Samouëlian A., Cousin I., Tabbagh A., Bruand A. and Richard G. 2005. Electrical resistivity survey in soil science: a review. *Soil and Tillage Research* **83**(2), 173–193.

Soupios P.M., Georgakopoulos P., Papadopoulos N., Saltas V., Andreadakis A., Vallianatos F. *et al.* 2007. Use of engineering geophysics to investigate a site for a building foundation. *Journal of Geophysics and Engineering* **4**, 94–103.

Soupios P.M., Loupasakis C. and Vallianatos F. 2008. Reconstructing former urban environments by combining geophysical electrical methods and geotechnical investigations - an example from Chania, Greece. *Journal of Geophysics and Engineering* **5**, 186–194.

Sudha K., Israil M., Mittal S. and Rai J. 2009. Soil characterization using electrical resistivity tomography and geotechnical investigations. *Journal of Applied Geophysics* **67**(1), 74–79.

Sultan S.A. and Santos F.A.M. 2007. 1D and 3D resistivity inversions for geotechnical investigation. *Journal of Geophysics and Engineering* **5**(1), 1.